



Structural, optical and electrical properties of zinc incorporated copper oxide nanoparticles: doping effect of Zn

R. O. Yathisha¹ and Y. Arthoba Nayaka^{1,*}

¹ Department of Chemistry, School of Chemical Sciences, Kuvempu University, Jnanasahyadri, Shankaraghatta, Karnataka 577 451, India

Received: 15 February 2017

Accepted: 22 August 2017

Published online:

11 September 2017

© Springer Science+Business Media, LLC 2017

ABSTRACT

The present paper demonstrates the effect of Zn ion doping on structural, electrical and optical properties of monoclinic CuO nanoparticles prepared via microwave combustion method. The crystal structure, optical and electrical properties of synthesized CuO and Zn-doped CuO samples were characterized by X-ray diffraction study, field emission scanning electron microscopy, energy-dispersive X-ray diffraction study, UV–Visible spectroscopy, transmission electron microscopy and photoconductivity technique. The XRD values show that the crystalline size of Zn-doped CuO nanoparticles was varied with Zn concentration and also it depends on the micro-strain and dislocation density of CuO lattice. FE-SEM and TEM images indicated that the synthesized samples are of the cube and rod-like structures in nature. The band gap of CuO nanoparticles has been calculated using Tauc's plot and the result showed that the incorporation of Zn has decreased the bandgap of CuO. The *I*–*V* characterization study was performed to determine the electrical property of CuO and Zn-doped CuO films. From the results, it is observed that the photocurrent of CuO and Zn-doped CuO films is found to be greater in UV-light as compared to dark.

Introduction

In recent years, the nanometer sized semiconducting metal oxides and transition metal-doped metal oxides have become subject of interest [1]. Currently, the research is focussed on the synthesis of various nanostructures of semiconducting metal oxides (such as nanorods, nanowires, nanoflowers, nanoprisms,

nanoplates, etc.), because of their structural dependent properties. In the oxides of copper family, cuprous oxide (Cu₂O) and cupric oxide (CuO) are the most selected metal oxides to prepare nanoparticles with different morphologies [2]. A number of CuO nanostructures have been synthesized in different morphologies through various methods like hydrothermal [3], solvothermal [4], co-precipitation

Address correspondence to E-mail: drarthoba@yahoo.co.in

[5], thermal evaporation [6], sonochemical [7] and sol–gel methods [8]. Generally, the above methods require technologically advanced equipments, additional solvents and consume more time for the preparation of CuO and transition metal-doped CuO nanoparticles [9]. Out of the various methods, microwave combustion method recently has been accepted as an efficient, faster and simple method for the synthesis of metal oxide nanoparticles. Because (i) microwaves have got strong penetrating power into the materials and hence increases the rate of reaction; (ii) the microwaves can be absorbed only by polarized material; (iii) microwave combustion is a “non-thermal” reaction. These conditions favor the acceleration in reaction rate, improvement of product yield, increased purity of material, good control of stoichiometry and well-defined size distribution [10]. Microwave combustion method has been used for the synthesis of nanoparticles such as CdO nanowires [11], CuS nanorods [12], platinum, gold, copper and ruthenium nanoprisms [13], spheres, flowers and stars like MgO [14] with novel properties.

Copper oxide is an important semiconducting transition metal oxide with a monoclinic crystal structure, and it has been studied as a *p*-type semiconducting metal oxide with a bandgap of 1.7 eV [15]. The CuO is being used as a novel material because of the ease of availability of raw materials, low processing cost, non-toxic nature, excellent thermal stability, good optical and electrical properties [16]. The unique physical, chemical and electrical properties of CuO nanoparticles have many potential applications in the fields of photo catalyst [17], batteries [18], gas sensing [19], solar cells [20] and biosensors [21]. It has been highlighted that the crystal shape and size are the two important considerations to control the optical and catalytic properties of CuO nanoparticles.

The doping is used to modify the optical and electrical properties of the host material by the addition of impurity ions into the lattice of the host material. Currently, an extensive research has been carried out to investigate the effect of doping elements such as Ni²⁺, Co^{2+/3+}, Zn²⁺, Cd²⁺, Cr^{2+/3+} and Fe^{2+/3+} on the electrical, optical and magnetic properties of CuO nanoparticles. Of all the transition metal ions, Zn²⁺ causes more effective doping with CuO since the ionic radius of Zn²⁺ (0.60 Å) and Cu²⁺ (0.57 Å) are similar to each other. Hence, Zn²⁺ ion can be easily incorporated into the CuO lattice

without destroying the crystal structure [22]. The conducting property of the nanomaterials depends upon the energy gap or band gap between the valance band and conduction band. It is possible to modify the conducting properties of CuO upon doping with Zn. A decrease in the band gap of CuO upon Zn doping has been reported by several authors. Jayaprakash et al. [23] have studied the effect of Zn doping on structural and optical properties of CuO and found that there is a decrease in the band gap of CuO upon doping with Zn. Rejith et al. [24] investigated the effect of incorporation of Zn on the bandgap of CuO.

In this research work, the synthesis of CuO and Zn-doped CuO nanoparticles ($0.00 \leq x \leq 0.10$) via microwave combustion method has been reported. The main goal of this work is to study the consequences of Zn doping on crystal structure, optical and electrical properties of CuO. The synthesized CuO and Zn-doped CuO nanoparticles have been characterized with the help of X-ray diffractometry (XRD), field emission scanning electron microscopy (FE-SEM), transmission electron microscopy (TEM), UV–Visible spectroscopy (UV–Vis) and photoconductivity techniques. The obtained results were discussed in terms of optical and electrical properties in correlation with crystal shape and size.

Experimental details

Materials

All the chemicals were purchased with the given analytical grades and used without further purification. Copper sulfate pentahydrate (CuSO₄·5H₂O, 99.5%, HiMedia), sodium hydroxide (NaOH, 98%, HiMedia), Urea (NH₂CONH₂, 99.5%, HiMedia) and zinc sulfate heptahydrate (ZnSO₄·7H₂O, 98%, Loba Chemie), acetone (CH₃COCH₃, ≥99%, Merck), absolute ethanol (C₂H₅OH, 99.9%, Changshu Yangshu Chemicals) were procured and used for the experiments as received. Double distilled water was used for the preparation of solutions. Domestic microwave Oven (Model: ONIDA POWER SOLD 17D, Power output-700 W, Frequency-2450 MHz) was used for the heating purposes.

Synthesis of CuO and Zn-doped CuO nanoparticles

In a typical synthesis, undoped CuO and Zn-doped CuO nanoparticles (0.0, 2.0, 4.0, 6.0, 8.0 and 10.0 at mol% of Zn) were prepared via microwave combustion method. For the preparation of CuO nanoparticles, an equimolar concentration (0.8 M each) of copper sulfate pentahydrate [CuSO₄·5H₂O] and urea (NH₂CONH₂) were dissolved in 100 ml of double distilled water. A 100 ml of 0.4 M sodium hydroxide solution was added drop-wise to the above mixture and kept stirring for 30 min at room temperature. When the solution turned blue to light green, 5 ml of this solution was taken in a china dish and placed in a domestic microwave oven. The solution was exposed to the microwave energy of 2450 MHz and 60% power (175 °C) for 8 min. Initially, the reaction solution was boiled and subsequently it underwent dehydration with the evolution of gases. The so obtained solid product was washed with double distilled water and absolute ethanol followed by acetone to remove the impurity ions like Na⁺, SO₄²⁻ and NH₄⁺, and dried at 80 °C for 5 h. It was finally calcinated at 600 °C for 2 h. The above procedure has been followed for the synthesis of Zn-doped CuO nanoparticles with the addition of ZnSO₄·7H₂O at different molar concentration.

Characterization of nanoparticles

The crystal structure and crystalline size of synthesized CuO and Zn-doped CuO nanoparticles were characterized by using high-resolution X-ray diffractometer (BRUKER: D8 Advance) provided with Cu-K α radiation at $\lambda = 0.154$ nm from an angle $2\theta = 30^\circ$ – 80° . The size distribution and morphology of the samples were analyzed by transmission electron microscope (TEM, Philips CM 200) and field emission scanning electron microscope fitted with an energy-dispersive analyzer using X-rays (FE-SEM, Carl Zeiss AG-ULTRA 55). The absorbance of CuO and Zn-doped CuO samples were measured on a UV-Vis spectrophotometer (USB 4000, Ocean Optics, USA). Photoconductivity studies were carried out using Keithley source meter with USB GRIB adaptor (Keithley – 2401).

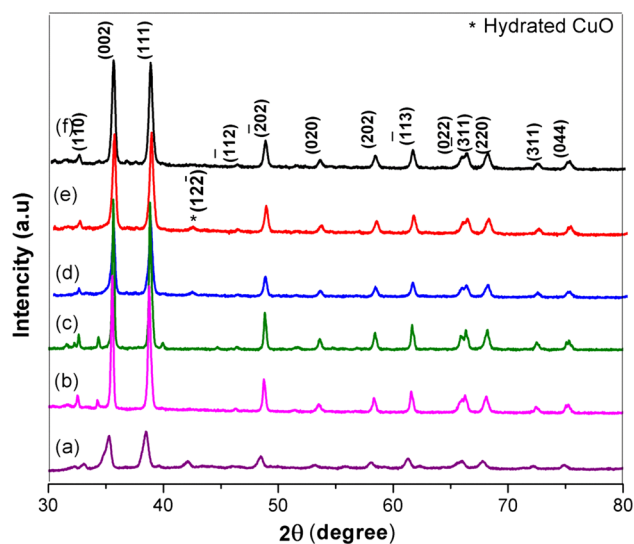


Figure 1 X-ray diffraction pattern of CuO and Zn-doped CuO ($0.00 \leq x \leq 0.10$) nanoparticles calcinated at 600 °C.

Results and discussion

XRD analysis

Figure 1 shows X-ray diffraction pattern of the CuO and Zn-doped CuO nanoparticles. The figure shows the phase purity and structural parameters of CuO and Zn-doped CuO nanoparticles ($0.00 \leq x \leq 0.10$, where 'x' represents molar concentration of dopant). The result shows a typical diffraction peaks at $2\theta = 32.52^\circ, 35.45^\circ, 38.76^\circ, 48.76^\circ, 53.50^\circ, 58.31^\circ, 61.56^\circ, 66.25^\circ, 68.12^\circ, 72.42^\circ$ and 75.25° , which correspond to (110), (002), (111), ($\bar{2}02$), (020), (202), ($\bar{1}13$), ($\bar{3}11$), (220), (311) and (044) Bragg's reflection planes of monoclinic (Tenorite) crystalline CuO (C_2/c symmetry group) according to JCPDS file No: 41-0254. A careful analysis of diffraction pattern shows that there is no trace of Zn related phases (metallic zinc, zinc oxide or binary zinc copper phases) or clusters for all Zn-doped CuO samples. This suggested that the dopants are well-integrated into the CuO lattice sites during the growth process. But the peak appeared in the 2θ range 40° – 45° may be attributed to the hydrated CuO according to JCPDS no. 42-0746. The appearance and disappearance of the peak positioned between 40° and 45° may be due to poorly differentiated ($12\bar{2}$) plane in the doped samples [25]. The CuO peaks were found to be broader as compared to Zn-doped CuO peaks. The diffraction plane ($\bar{2}02$) was narrower than (002) plane, and (002) in

turn was narrower than (111) plane. This clearly indicated the existence of asymmetry in the crystalline shape and synthesized materials are in the nanometer range [26]. To confirm the substitution of Zn²⁺ ions in place of Cu²⁺ ions in Zn-doped CuO nanoparticles, the shift of angle (2θ) along major (111) and (002) diffraction planes as a function of doping was observed. These data reveals that the positions of peaks slightly shifted toward the right side up to 4 mol% of Zn and on further increase in the doping percentage, the peaks were slightly shifted toward the left side of the graph (Fig. 2a). This is because the Zn substitution does not acutely change the lattice constants of CuO, it can bring about residual stress which may lead to anisotropic shrinkage of lattices and then produces lattice distortion. Pressure stress can cause diffraction planes shift to higher angles, whereas tensile stress results in the shift of lower angle [27]. The deviation in the diffraction angle indicated that the microstructure and crystalline size of Zn-doped CuO nanoparticles are dependent on the percentage of Zn doping. Also, with increase in Zn content up to 4 mol%, the peak intensity of (111) and (002) planes has been increased (Fig. 1b, c) and above 4 mol% of Zn in CuO lattice has resulted in the broadening of FWHM with a subsequent decrease in

the peak intensity (Fig. 1d, e) [28]. The lattice parameters for CuO and Zn-doped CuO were calculated from XRD data. It reveals that there is no linear dependence of the lattice parameters with the concentration of Zn content [29]. This can be explained on the basis of the replacement of larger ionic radius Zn²⁺ ion (0.60 Å) with smaller ionic radius Cu²⁺ ion (0.57 Å) [30]. The lattice parameters for the monoclinic structure of CuO and Zn-doped CuO nanoparticles ($x \neq y \neq z, \alpha = \gamma = 90^\circ \neq \beta$) were calculated using the equation based on Bragg's law ($2d\sin\theta = n\lambda$):

$$\frac{1}{d^2} = \frac{1}{\sin^2 \beta} \left(\frac{h^2}{x^2} + \frac{k^2 \sin^2 \beta}{y^2} + \frac{l^2}{z^2} - \frac{2hl \cos \beta}{xz} \right) \quad (1)$$

where x, y and z are the lattice constants, d is the interplanar spacing, β is the interfacial angle and h, k, l are the Miller indices [31].

Figure 2b shows the decrease in full width at half maxima (FWHM) for Zn-doped CuO nanoparticles as compared to pure CuO nanoparticles (Table 1). This is due to the crystalline size induced or micro-strain induced reduction, since (111) and (002) peaks positions almost have changed as shown in Fig. 2a, [32].

The crystalline size (D), dislocation density (δ) and micro-strain (ϵ) of CuO and Zn-doped CuO

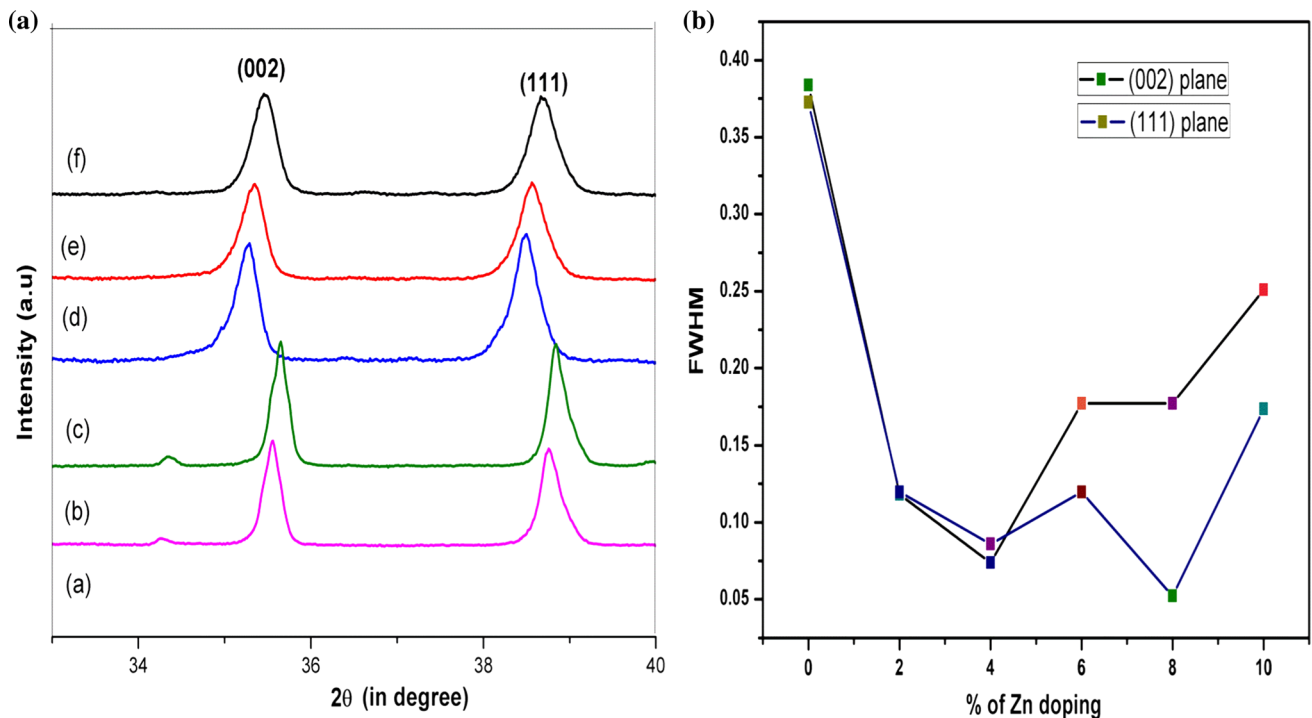


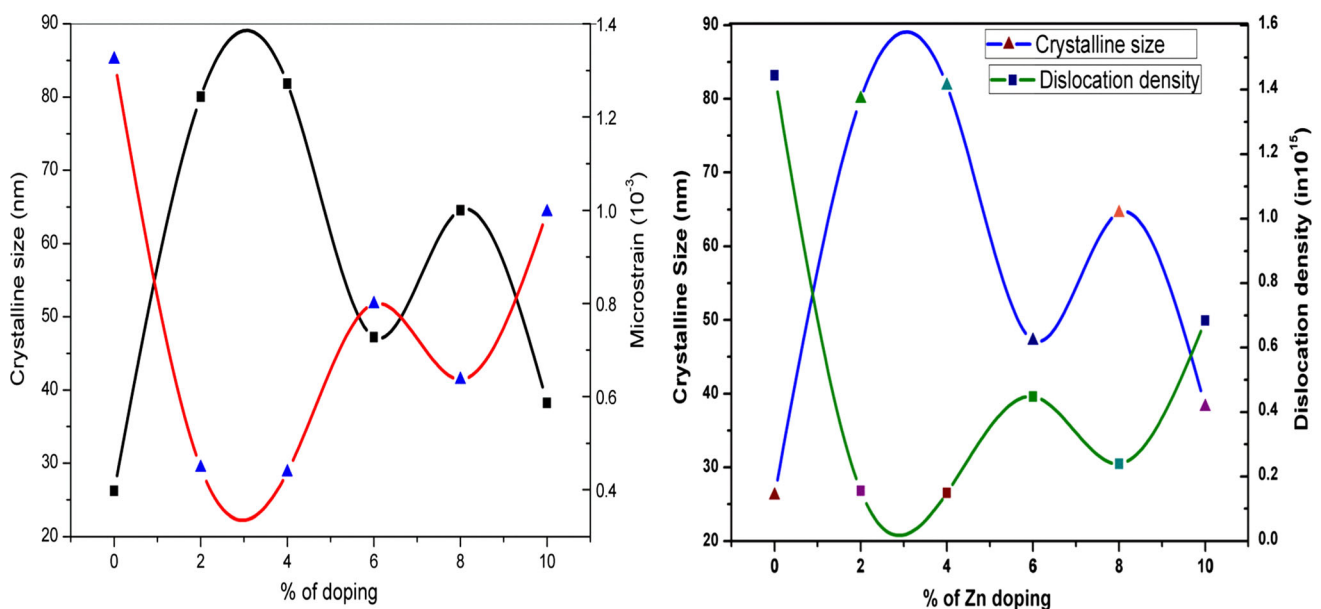
Figure 2 **a** The shift of peak position of CuO and Zn-doped CuO ($0.00 \leq x \leq 0.10$) nanoparticles, **b** the change in the FWHM of CuO with different Zn concentration.

Table 1 The variation of peak position (2θ), full width at half maxima (FWHM), d -values at (002) and (111) planes

% of Zn doping	2θ ($^\circ$)	(h k l)	FWHM (β in degree)	d (\AA)
CuO	35.2663	(002)	0.3838	2.5450
	38.4923	(111)	0.3542	2.3388
Cu _{0.98} Zn _{0.02} O	35.5545	(002)	0.1181	2.5250
	38.8880	(111)	0.1328	2.3140
Cu _{0.96} Zn _{0.04} O	35.6475	(002)	0.0738	2.5059
	38.8372	(111)	0.1031	2.3188
Cu _{0.94} Zn _{0.06} O	35.2751	(002)	0.1771	2.5443
	38.4932	(111)	0.1328	2.3307
Cu _{0.92} Zn _{0.08} O	35.3503	(002)	0.1771	2.5309
	38.5667	(111)	0.0738	2.3344
Cu _{0.90} Zn _{0.10} O	35.4692	(002)	0.2509	2.5309
	38.6896	(111)	0.1800	2.3254

Table 2 Calculated values of lattice parameters, cell volume, average crystalline size, micro-strain and dislocation density

Property	CuO	Cu _{0.98} Zn _{0.02} O	Cu _{0.96} Zn _{0.04} O	Cu _{0.94} Zn _{0.06} O	Cu _{0.92} Zn _{0.08} O	Cu _{0.90} Zn _{0.10} O
x (\AA)	4.7174	4.6909	4.6807	4.7126	4.6968	4.7030
y (\AA)	3.4321	3.4262	3.4204	3.4366	3.4270	3.4357
z (\AA)	5.1465	5.1302	5.1265	5.1464	5.1282	5.1443
β ($^\circ$)	99.693	99.522	99.500	99.628	99.552	99.596
Cell volume (\AA^3)	82.1388	81.3164	80.9529	82.1748	81.3987	81.9590
Average crystalline size from XRD (nm)	26.21	80.04	81.83	47.24	64.57	38.23
Micro-strain (ϵ) in $\times 10^{-3}$	1.3242	0.4475	0.4380	0.7992	0.6367	0.9965
Dislocation density (δ) in $\times 10^{15}$	1.4556	0.1561	0.1494	0.4481	0.2398	0.6842

**Figure 3** Inter-relation between crystalline size, micro-strain and dislocation density of CuO and Zn-doped CuO ($0.00 \leq x \leq 0.10$) nanoparticles calculated at 600 $^\circ\text{C}$.

nanoparticles were calculated and are given in Table 2. Figure 3 is clearly indicating that the micro-strain is directly proportional to the dislocation

density and inversely proportional to the crystalline size. Dislocations are the irregularity in a crystal which arises due to the lattice mismatch from one

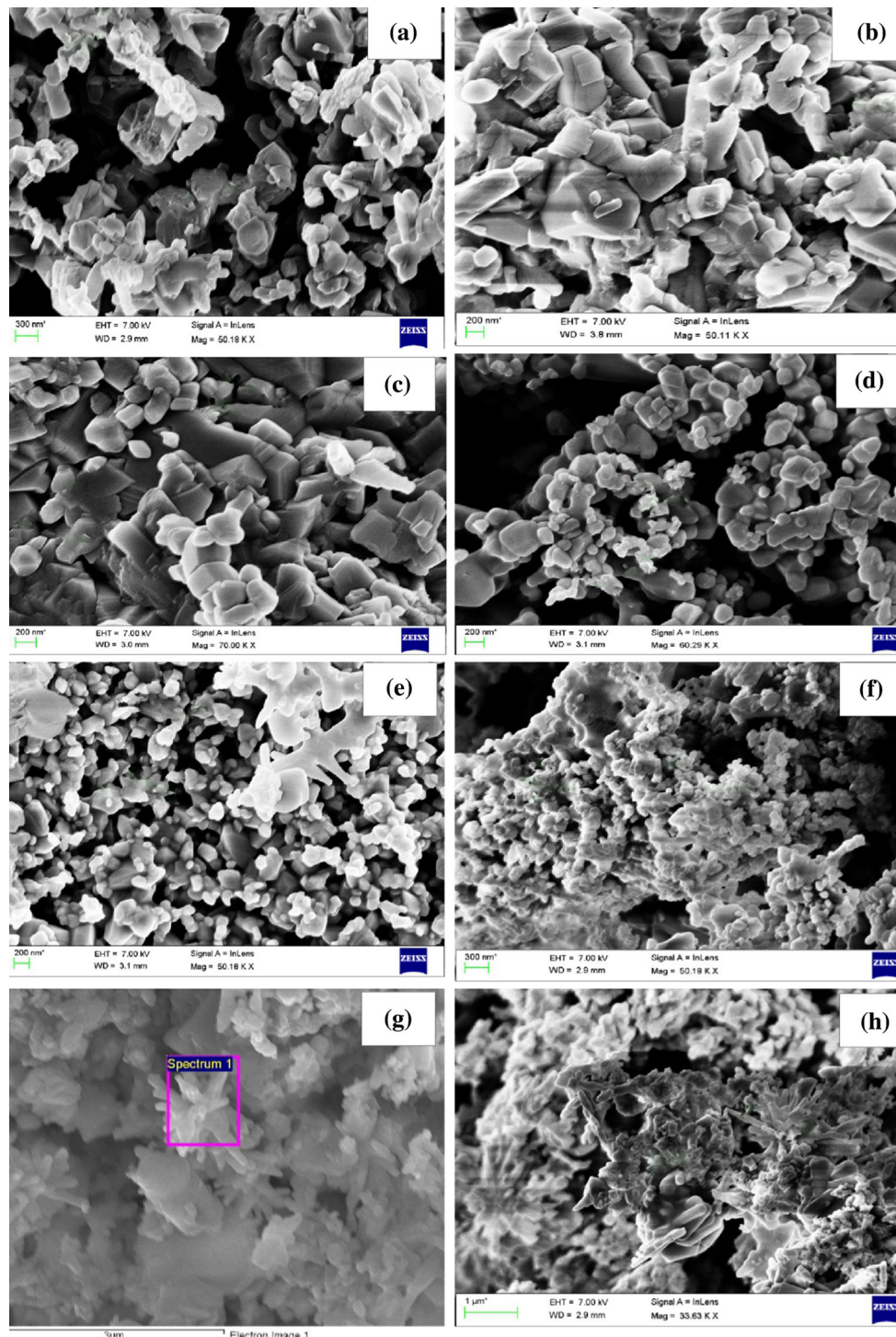


Figure 4 FE-SEM images of **a** undoped CuO, **b** 2 mol% of Zn-doped CuO, **c** 4 mol% of Zn-doped CuO, **d** 6 mol% of Zn-doped CuO, **e** 8 mol% of Zn-doped CuO, **f** 10 mol% of Zn-doped CuO,

g, h flower-shaped agglomerated Zn-doped CuO nanoparticles (8 and 10 mol%).

part of the crystal to another part. In this case, the dislocation densities are found to vary along with micro-strain as shown in Fig. 3a, b [33]. The average

crystalline size of CuO and Zn-doped CuO nanoparticles were calculated from the Scherrer's formula [34]:

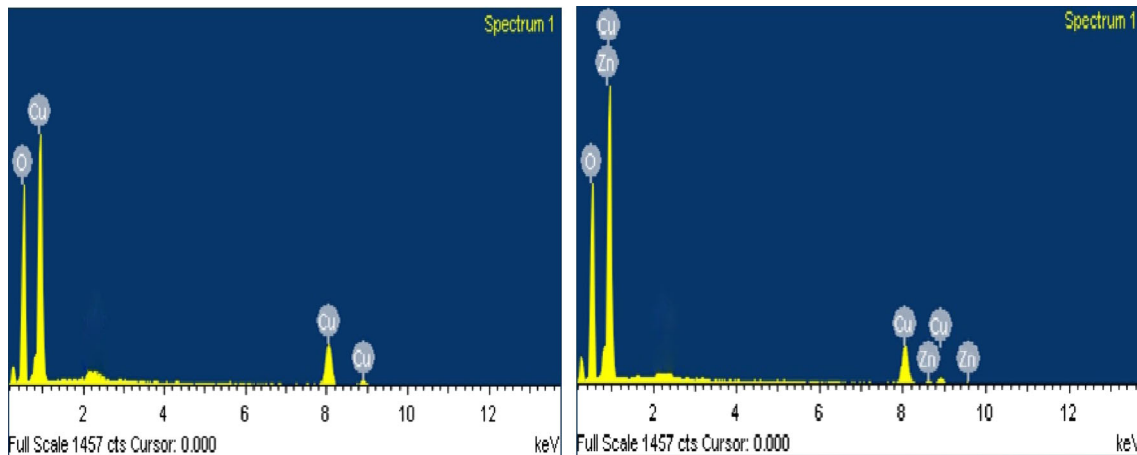


Figure 5 EDAX spectra of undoped CuO and 8 mol% Zn-doped CuO nanoparticles.

Table 3 The atomic percentage ratio of Cu, Zn and O in CuO and Zn-doped CuO nanoparticles

Samples ratio	Atomic (%) percentage of the elements			
	Cu	O	Zn	Zn/Cu
CuO	27.93	72.07	–	–
Cu _{0.92} Zn _{0.08} O	30.45	67.10	2.45	0.0804

$$\text{Average crystallite size } (D) = \frac{0.9\lambda}{\beta \cos \theta} \quad (2)$$

where λ is the wavelength of X-ray used (0.154 nm), β is the full width at half maximum in radians and θ is the Bragg's diffraction angle. The micro-strain, unit cell volume and dislocation density have been calculated from the following equations:

$$\text{Micro-strain } (\varepsilon) = \frac{\beta \cos \theta}{4} \quad (3)$$

$$\text{Unit cell volume } (V) = xyz (\sin \beta) \quad (4)$$

$$\text{Dislocation density } (\delta) = \frac{1}{D^2} \quad (5)$$

where, β is the full width at half maximum in radians, x , y and z are the lattice parameters, and β is the interfacial angle, D is the crystalline size in nm [35, 36].

SEM and EDAX analysis

The morphological characteristics of CuO and Zn-doped CuO ($0.00 \leq x \leq 0.10$) nanoparticles are shown in Fig. 4a–h. Figure 4a shows SEM

photomicrograph of synthesized CuO nanoparticles. The image shows that the metal oxide has got a mixture of cubes and rod-like structures with an uneven grain size of 21–100 nm with a better crystalline quality. This is due to the anisotropic growth of monoclinic CuO crystal consisting of alternately arranged O^{2-} and Cu^{2+} ions along the specific directions [37]. In general, Zn doping does not have much influence on the morphology of CuO. But upon Zn doping, variation in the size of the CuO nanoparticles with the formation of elongated and small nanostructures has been observed. Figure 4g, h shows the low magnification FE-SEM images of flower-shaped Zn-doped CuO nanostructures. Being NaOH is a strong electrolyte, neutralizes the surface charges of Zn-doped CuO which affects the aggregation. In the current experimental results, NaOH showed significant results in aggregating the individual particles. Moreover, it is also shown that the flower- and spherical-like assemblies of Zn-doped CuO have the strong binding energy between individual particles due to the electrostatic force of attraction. Therefore, it is expected that the electrostatic force of attraction also plays an important role in the development of flower-like nanostructures by the assemblage of individual particles. The XRD data revealed that the average size of the particles has been increased up to 4 mol% of Zn and a further increase in the concentration, the size of the particles was found to be varied irregularly due to the induction of micro-strain and lattice mismatch in the lattice [38]. This can also be observed in the SEM photomicrographs. Figure 5 shows the EDAX spectra of pure CuO and 8 mol% Zn-doped CuO

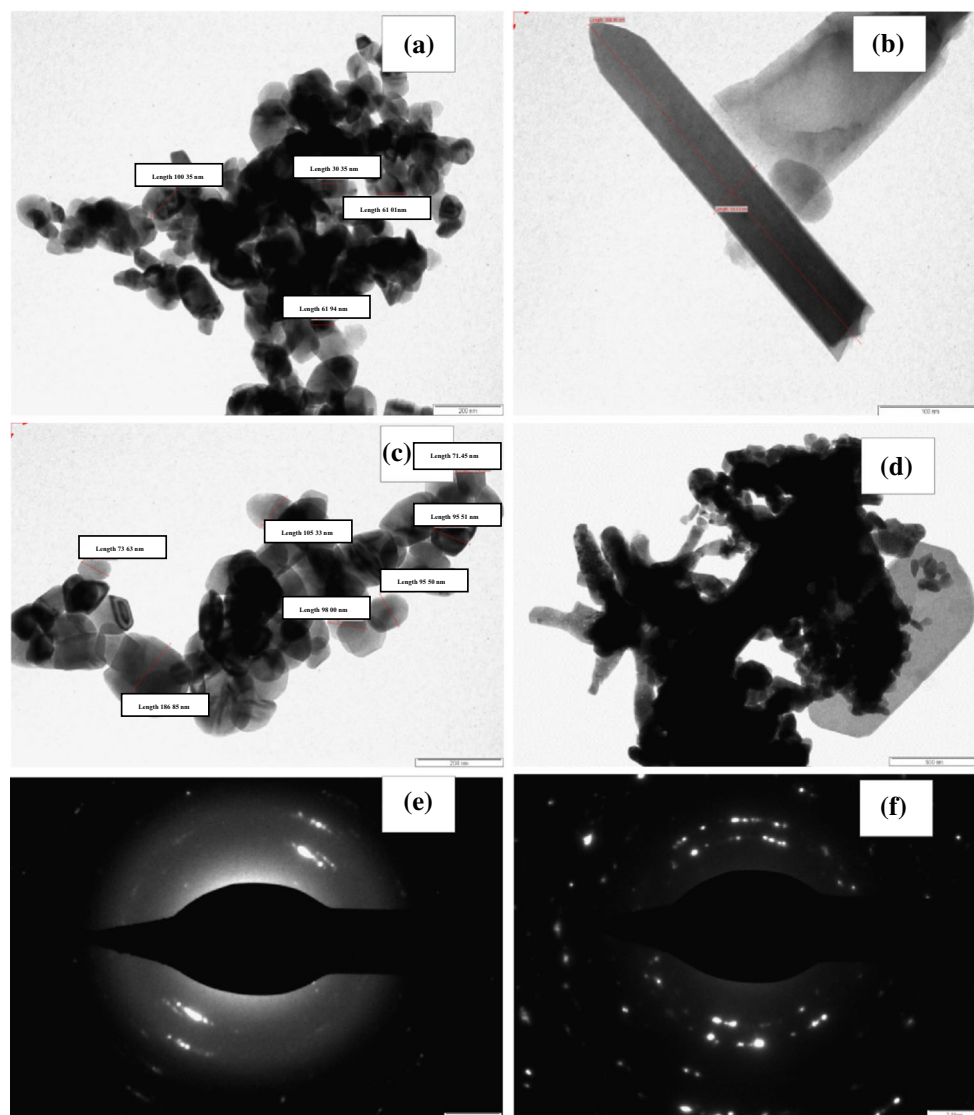


Figure 6 TEM images and SAED pattern of undoped CuO and 8 mol% Zn-doped CuO nanoparticles calcinated at 600 °C.

nanoparticles. The EDAX analysis of Zn-doped CuO nanoparticles confirms the presence of Zn in CuO lattice. The calculated atomic percentage of compositional elements such as Zn, Cu and O present in CuO and 8 mol% Zn-doped CuO nanoparticles are given in Table 3. The quantitative atomic percentage of Zn/Cu ratio was found to be 0.0804 mol (8.04 mol%) in 8 mol% of Zn-doped CuO nanoparticles. The EDAX spectrum confirms the existence of Zn ions in Zn-doped CuO nanoparticles, and the atomic percentage of Zn is almost identical to their usual stoichiometry within the experimental error. Therefore, the EDAX spectrum shows a good agreement with the experimental results [39].

TEM and SAED analysis

Figure 6a–f shows the transmission electron microscopic (TEM) images and selected area electron diffraction (SAED) images for CuO and Zn-doped CuO (8 mol% of Zn) nanoparticles synthesized via microwave combustion method and annealed at 600 °C. Figure 6a, c shows the cube-like structures of CuO and Zn-doped CuO nanoparticles with different particle size. Figure 6b shows the rod-shaped CuO nanocrystals of length 386.45 nm and breadth 59.40 nm. For both CuO and 8 mol% Zn-doped CuO nanoparticles, the agglomeration of crystals has been observed. The extent of agglomeration is small in pure CuO as compared to 8 mol% of Zn-doped CuO

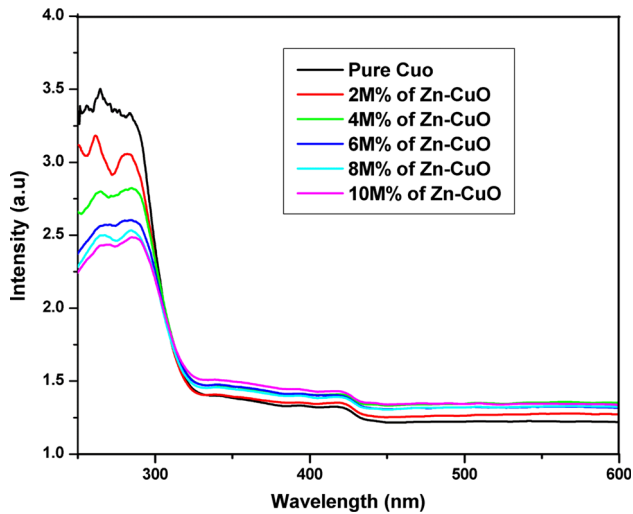


Figure 7 UV–Visible spectra of CuO and Zn-doped CuO ($0.00 \leq x \leq 0.10$) nanoparticles.

nanoparticles. Figure 6d shows the agglomeration of individual Zn-doped CuO nanoparticles forming flower-shaped nanostructures. The particles size have been calculated from TEM images and are found to be in the range of 30–100 nm for CuO and 71–186 nm for 8 mol% Zn-doped CuO nanoparticles [40]. The SAED pattern of CuO and Zn-doped CuO is shown in Fig. 6e, f. The SAED pattern of CuO (Fig. 6e) shows diffused rings, indicating that the synthesized material is polycrystalline in nature. On the other hand, SAED pattern of Zn-doped CuO (Fig. 6f) confirmed the formation of well-defined single phase crystal with monoclinic structure. Hence, the results of SAED also support the experimental evidences observed from the XRD results [41].

UV–Vis spectral analysis

Figure 7 shows the optical properties of CuO and Zn-doped CuO nanoparticles. The UV–Vis spectra have been recorded in the wavelength range 300–800 nm at room temperature. The absorption spectrum has been used to derive the optical bandgaps of CuO and Zn-doped CuO nanoparticles. The direct band gap of CuO nanoparticles has been found to be 2.31 eV. The increase in the bandgap of synthesized nanoparticles as compared to that of its bulk counterpart (1.85 eV) could be attributed to the quantum size effect [42]. In the case of bulk matter, the energy bands between the different energy states are actually formed by the

combination of a group of adjacent energy levels of several atoms. As the particle size approaches the nanoscale dimension, the overlapping of adjacent energy levels minimizes and subsequently the width of energy band gets widen. Hence, the energy gap between the valence band and conduction band increases as the particle size decreases. Upon doping of Zn up to 2–4 mol%, the optical absorption edge has slightly shifted toward longer wavelength (2.17–2.12 eV) and on further increase in Zn content, the absorption edge has shifted toward shorter wavelength (2.21–2.25 eV). This attribution of absorbance mainly depends upon some of the factors like particle size, oxygen deficiency, lattice strain and thickness etc. [43]. The optical band gap (E_g) of pure CuO and Zn-doped CuO is derived from the Tauc's formula, $(\alpha h\nu)^{1/n} = A (h\nu - E_g)$, where h is Planks constant (6.626×10^{-34} J s), A is an energy-independent constant, α is the absorption coefficient, E_g is the optical bandgap of valence and conduction band (eV) and n is determined the optical transition of semiconductor. On plotting the values of $(\alpha h\nu)^2$ versus $h\nu$, a better linearity has been observed for the direct transition (Fig. 8). The band gap of Zn-doped CuO with different concentration of Zn was found to be 2.17, 2.12, 2.23, 2.21 and 2.25 eV for 2, 4, 6, 8 and 10 mol%, respectively [44, 45]. According to Wang et al. statement, absorption band energy E_g and crystalline size D are found to be inversely dependent. The relationship between the optical band gap and crystallite size is shown by the formula:

$$E(R) = E_g(\infty) + E_b \left(\frac{\pi m_B}{R} \right)^2 \quad (6)$$

where $E_g(\infty)$ is the band gap energy (eV), E_n is the exciton binding energy, and m_B is the exciton Bohr radius which appears in the range of 6.6–28.7 nm. Both E_n and m_B are constant for CuO [46].

Electrical properties

The current and resistance are the two parameters play an important role in the investigation of electrical properties of conducting materials [47]. According to Ohm's law, the current in a circuit is directly proportional to the voltage across the circuit and inversely proportional to the total resistance in the circuit [48]. The I – V characteristic studies of CuO and Zn-doped CuO films have been carried out using silver paste to make good electrical contact.

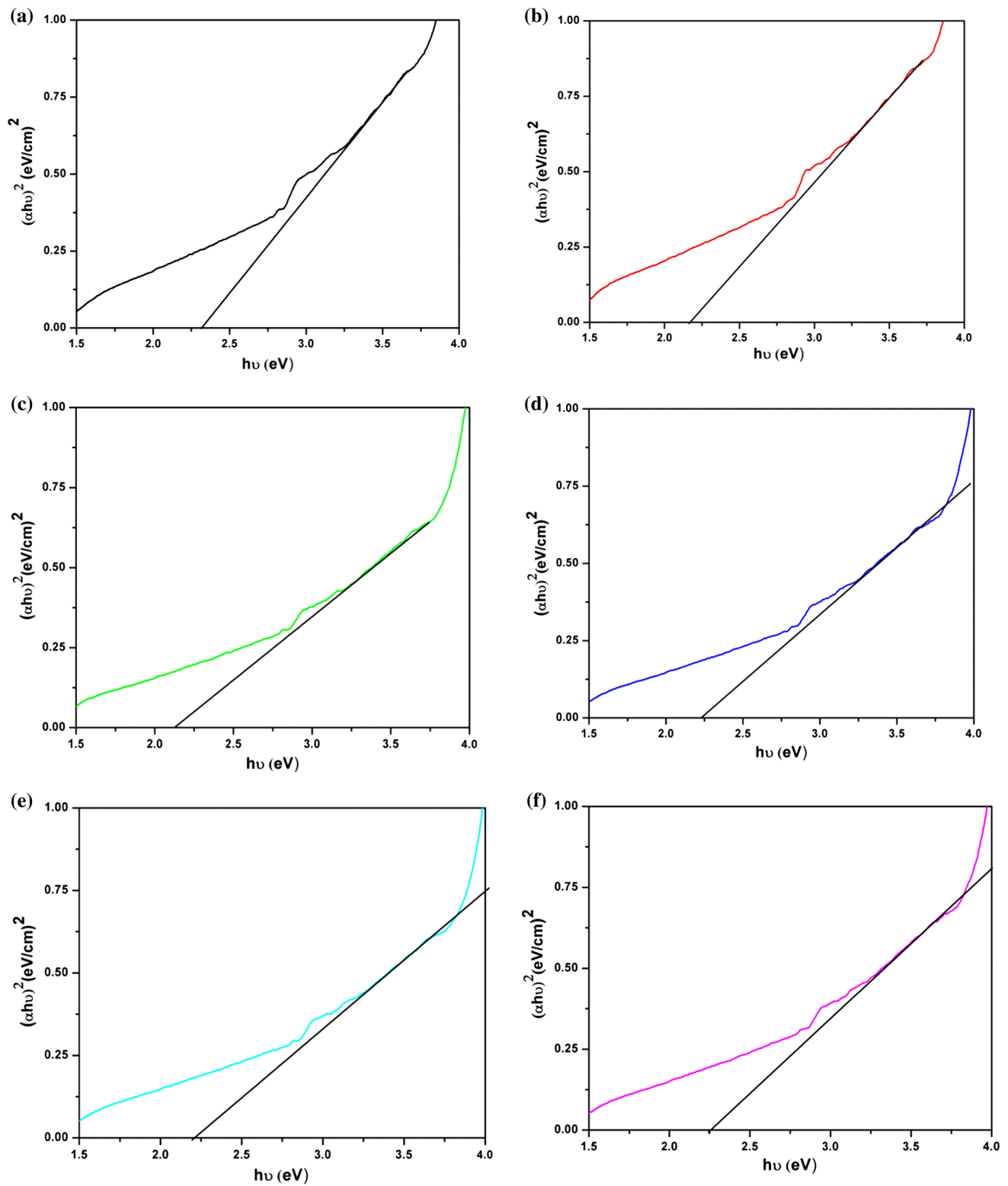


Figure 8 Tauc's plot of **a** undoped CuO, **b** 2 mol% of Zn-doped CuO, **c** 4 mol% of Zn-doped CuO, **d** 6 mol% of Zn-doped CuO, **e** 8 mol% of Zn-doped CuO and **f** 10 mol% of Zn-doped CuO nanoparticles.

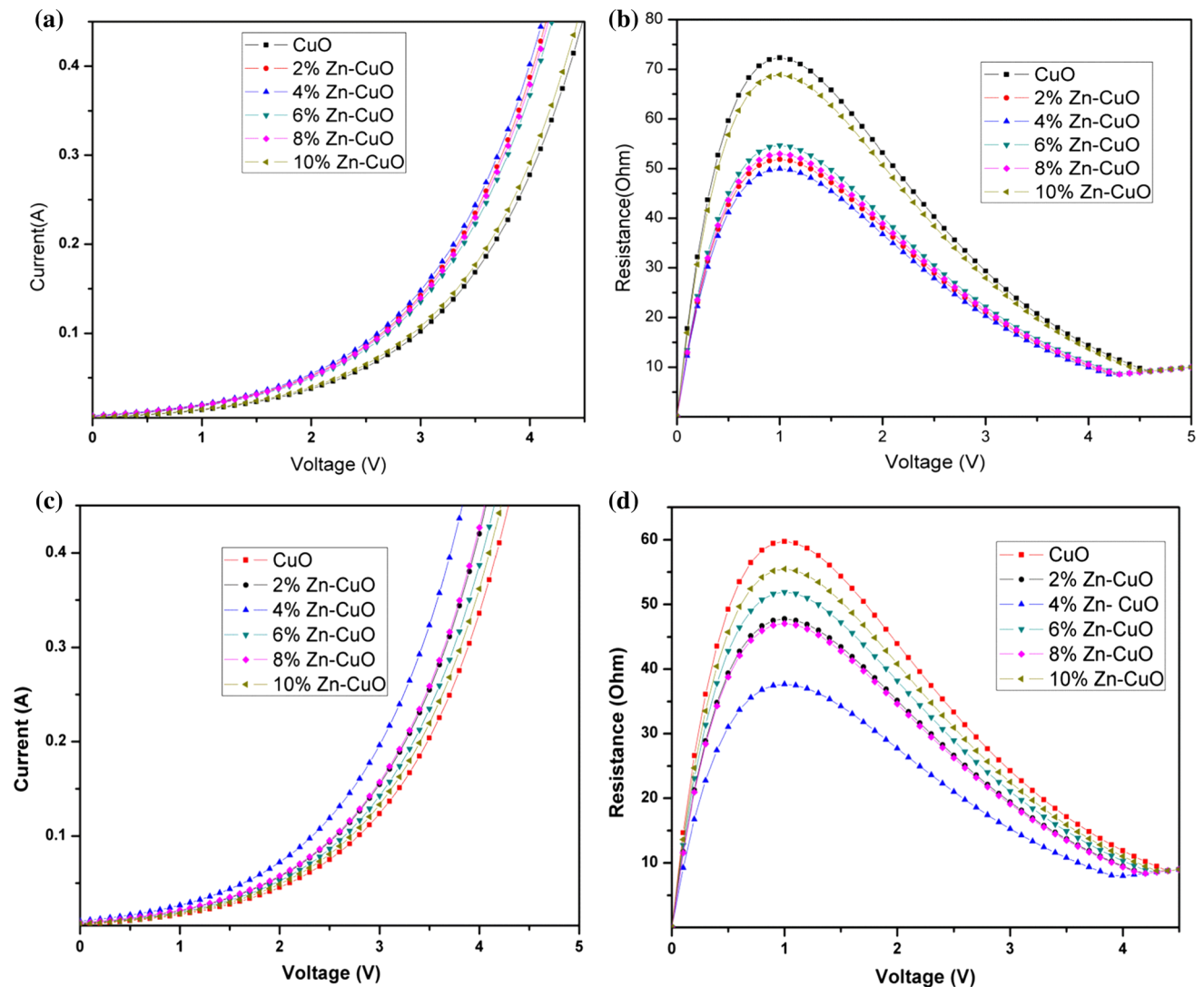


Figure 9 I - V characteristics of undoped CuO and Zn-doped CuO in *dark* condition (a, b) and *light* condition (c, d), calcinated at 600 °C.

Table 4 The variation of conductance and resistance with band gap in the dark and UV-light conditions (at 4 V)

%Zn doping	Band gap (eV)	Dark condition		Light condition	
		Current (A)	Resistance (Ω)	Current (A)	Resistance (Ω)
CuO	2.31	0.2778	14.3999	0.3361	11.8998
$\text{Cu}_{0.98}\text{Zn}_{0.02}\text{O}$	2.17	0.3874	10.3245	0.4204	09.5140
$\text{Cu}_{0.96}\text{Zn}_{0.04}\text{O}$	2.12	0.4019	09.9528	0.5000	08.0000
$\text{Cu}_{0.94}\text{Zn}_{0.06}\text{O}$	2.23	0.3675	10.2886	0.3870	10.3359
$\text{Cu}_{0.92}\text{Zn}_{0.08}\text{O}$	2.21	0.3794	10.5418	0.4268	09.3702
$\text{Cu}_{0.90}\text{Zn}_{0.10}\text{O}$	2.25	0.2915	13.7202	0.3620	11.0490

Figure 9a–d shows the I - V characteristics of CuO and Zn-doped CuO under the dark and UV-light condition. From the I - V curves, it can be seen that the pure CuO sample shows very high resistance in the dark condition. This may be due to the effect of grain

boundaries on the mobility of charge carriers. These boundaries act as dissemination sites and potential walls which lead to a reduction in the carrier mobility by increasing the resistance and decreasing the current [49]. At low concentration of Zn doping

(2–4 mol%) into CuO lattice, the decrease in resistance is due to the replacement of Cu^{2+} ($3d^9$) ions by Zn^{2+} ($3d^{10}$) ions which introduce a number of electrons in the doped films, thus the charge carriers. Hence, the conductivity of Zn-doped CuO films has been enhanced. However, with further increase in the doping concentration of Zn, a slight increase in the resistance was observed. This reduction in conductance at higher concentration of Zn dopant could be attributed to the segregation of Zn ions in the grain boundaries. Moreover, at higher concentration of Zn, the neutral defect may be observed. As a result of these defects, the excess charge carriers get neutralize and leads to an increased resistivity [50]. The prepared CuO and Zn-doped CuO films have shown a considerable enhancement in the conductivity under UV-light condition. This indicated that the motion of charge carriers increases under the light condition and considerably improves the conduction of CuO and Zn-doped CuO films [51]. The remarkable increase in the conductance by these samples may result in higher efficiency of the solar cells [52, 53]. The measured band gap, conductance and resistance for CuO and Zn-doped CuO (at 4 V) are given in Table 4.

Conclusion

In the present work, synthesis of CuO and Zn-doped CuO nanoparticles via simple microwave combustion method has been reported. The effect of Zn doping on the structural, optical and electrical properties of CuO nanoparticles have been studied. The SEM and TEM analysis revealed that the size and morphology of Zn-doped CuO nanoparticles depend on the concentration of Zn dopant. The optical properties of synthesized nanoparticles were studied by measuring of band gap energy. This reveals that with increasing the doping concentration of Zn up to 4 mol%, the band gap edge shifted to longer wavelength region. The I – V characteristic studies of CuO and Zn-doped CuO films in dark and under UV-light illumination have shown the dependency between the conduction and the concentration of dopant. Therefore, estimated optical band gap energy, conductance and resistance of Zn-doped CuO are very useful for the applications in the solar cells and optical devices.

Acknowledgements

Authors are grateful to SERB, New Delhi, for providing financial support in the form of Major Research Project. The authors are also thankful to Indian Institute of Science, Bangalore and SAIF Bombay for the support to carry out this work.

References

- [1] Mote VD, Dargad JS, Purushotham Y, Dole BN (2015) Effect of doping on structural, physical, morphological and optical properties of $\text{Zn}_{1-x}\text{Mn}_x\text{O}$ nano-particles. *Ceram Int* 41:15153
- [2] Fuku X, Kaviyarasu K, Matinise M, Maaza M (2016) Punicalagin green functionalized Cu/Cu₂O/ZnO/CuO nanocomposite for potential electrochemical transducer and catalyst. *Nanoscale Res Lett* 11:386
- [3] Outokesh K, Hosseinpour M, Ahmadi SJ, Mousavand T, Sadjadi S, Soltanian W (2011) Hydrothermal synthesis of CuO nanoparticles: study on effects of operational conditions on yield, purity, size of the nanoparticles. *Ind Eng Chem Res* 50:3540
- [4] Wang T, Xiao Q (2013) Solvothermal synthesis and sensing properties of meso-macroporous hierarchical CuO microspheres composed of nanosheets. *Mater Chem Phys* 139:603
- [5] Li L, Mao D, Yu J, Guo X (2015) Highly selective hydrogenation of CO₂ to methanol over CuO–ZnO–ZrO₂ catalysts prepared by a surfactant-assisted co-precipitation method. *J Power Sources* 279:394
- [6] Khalaji AD, Jafari K, Rad SM (2013) Solid-state thermal decomposition method for the preparation of CuO nanoparticles. *J Nan Str* 2:505
- [7] Sonia S, Jayram ND, Kumar PS, Mangalaraj D, Ponpandian N, Viswanathan C (2014) Effect of NaOH concentration on structural, surface and antibacterial activity of CuO nanorods synthesized by direct sonochemical method. *Super lattices Microstruct* 66:1
- [8] Yahia IS, Farag AAM, El-Faify S, Yakuphanoglu F, Al-Ghamdi AA (2016) Synthesis, optical constants, optical dispersion parameters of CuO nanorods. *Optik* 127:1430
- [9] Selvam NCS, Kumar RT, Yogeenth K, Kennedy LJ, Sekaran G, Vijaya JJ (2011) Simple and rapid synthesis of cadmium oxide (CdO) nanospheres by a microwave-assisted combustion method. *Pow Technol* 211:250
- [10] Jing S, Wang W, Yue Q, Chunyuan M, Zhang J, Zhao X, Song Z (2016) Review on microwave–metal discharges and their applications in energy and industrial processes. *Appl Energy* 175:142

- [11] Eskizeybek V, Avci A, Chhowalla M (2011) Structural and optical properties of CdO nanowires synthesized from Cd(OH)₂ precursors by calcinations. *Cryst Res Technol* 46:1093
- [12] Dhasade SS, Patil JS, Kim JH, Han SH, Rath MC, Fulari VJ (2012) Synthesis of CuS nanorods grown at room temperature by electrodeposition method. *Mater Chem Phys* 137:353
- [13] Harada M, Cong C (2016) Microwave-assisted polyol synthesis of polymer-protected monometallic nanoparticles prepared in batch and continuous-flow processing. *Ind Eng Chem Res* 55:5635
- [14] Kashif M, Hashim U, Ali AE, Usman Ali SM, Rusop M, Ibpoto ZH, Willander M (2012) Effect of different seed solutions on the morphology and electrooptical properties of ZnO nanorods. *J Nanomater* 2012:2
- [15] Jiang T, Wang Y, Meng D, Wu X, Wang J, Chen J (2014) Controllable fabrication of CuO nanostructure by hydrothermal method and its properties. *Appl Surf Sci* 311:602
- [16] El-Trass A, Shamy HE, Mehasseb IE, Kemary ME (2012) CuO nanoparticles: synthesis, characterization, optical properties and interaction with amino acids. *Appl Surf Sci* 258:2997
- [17] Sharma A, Varshney M, Kyun HT, Chae KH, Shin HJ (2015) X-ray absorption spectroscopy study and photocatalyst application of CuO and Cu_{0.9}Ti_{0.1}O nanoparticles. *Curr Appl Phys* 15:1148
- [18] Li X, Guo W, Liu Y, He W, Xiao Z (2014) Spinel LiNi_{0.5}Mn_{1.5}O₄ as superior electrode materials for lithium-ion batteries: Ionic liquid assisted synthesis and the effect of CuO coating. *Electrochimica Acta* 116:278
- [19] Lee J, Katoch A, Kim J, Kim S (2016) Effect of Au nanoparticle size on the gas-sensing performance of p-CuO nanowires. *Sens Actuators B Chem* 222:307
- [20] Siddiqui H, Qureshi MS, Haque FZ (2016) Valuation of copper oxide (CuO) nanoflakes for its suitability as an absorbing material in solar cells fabrication. *Optik* 127:3713
- [21] Etefagh R, Azhir E, Shahtahmasebi N (2013) Synthesis of CuO nanoparticles and fabrication of nanostructural layer biosensors for detecting *Aspergillus niger* fungi. *Sci Iran F* 20(3):1055
- [22] Kumar MA, Kumaran SM (2015) Effect of Ni doping on electrical, photoluminescence and magnetic behaviour of Cu doped ZnO nanoparticles. *J Lumin* 162:97
- [23] Jayaprakash J, Srinivasan N, Chandrasekaran P, Girija EK (2015) Synthesis and characterization of cluster of grapes like pure and Zinc doped CuO nanoparticles by sol-gel method. *Spect Acta Part A Mol Biomol Spect* 136:1804
- [24] Rejith SG, Krishnan C (2013) Optical characterizations of Zn doped CuO nanoparticles. *Mater Lett* 106:88
- [25] Conghua Lu, Qi Limin et al (2004) Simple template-free solution route for the controlled synthesis of Cu(OH)₂ and CuO nanostructures. *J Phys Chem B* 108:17826–17827
- [26] El Mir L, Ayadi ZB, Rahmouni H, El Ghoul J, Djessas K, Bardeleben HJV (2009) Elaboration and characterization of Co doped, conductive ZnO thin films deposited by radio-frequency magnetron sputtering at room temperature. *Thin Solid Films* 517:6008
- [27] Ansari SA, Nisar A, Fatma B, Khan W, Naqvi AH (2012) Investigation on structural, optical and dielectric properties of Co doped ZnO nanoparticles synthesized by gel-combustion route. *Mater Sci Eng B* 177:429
- [28] Vidyasagar CC, Muralidhara HB, Naik YA, Hosamani G, Ilango MS (2015) Effect of annealing on structural, crystallinity and optical properties of anatase Cr-TiO₂ nanoparticles. *Energy Environ Focus* 4:3
- [29] Jiang T, Wang Y, Meng D, Wang D (2016) One-step hydrothermal synthesis and enhanced photocatalytic performance of pine-needle-like Zn-doped CuO nanostructures. *J Mater Sci Mater Electron* 27:12885
- [30] Yildirim OA, Durucan C (2016) Room temperature synthesis of Cu incorporated ZnO nanoparticles with room temperature ferromagnetic activity: structural, optical and magnetic characterization. *Ceram Int* 42:3232
- [31] Singh I, Kaur G, Bedi RK (2011) CTAB assisted growth and characterization of nanocrystalline CuO films by ultrasonic spray pyrolysis technique. *Appl Surf Sci* 257:9550
- [32] Viruthagiri G, Praveen P, Mugundan S, Gopinathan E (2013) Synthesis and characterization of pure and nickel doped Sr-TiO₃ nanoparticles via solid state reaction route. *Ind J Adv Chem Sci* 1(3):134
- [33] Venkateswarulu K, Sandyarani M, Nellaippan TA, Rameshbabu N (2014) Estimation of crystalline size, Lattice strain and dislocation density of nanocrystalline carbonate substituted hydroxyapatite by X-ray peak variance analysis. *Proc Mater Sci* 5:218
- [34] Vidyasagar CC, Arthoba Naik Y, Venkatesh TG, Viswanatha R (2011) Solid state synthesis and effect of temperature on optical properties of Cu-ZnO, Cu-CdO and CuO nanoparticles. *Powder Technol* 214:339
- [35] Singh I, Bedi RK (2011) Studies and correlation among the structural, electrical and gas response properties of aerosol spray deposited self assembled nanocrystalline CuO. *Appl Surf Sci* 257:7595
- [36] Raja K, Ramesh PS, Geetha D (2014) Structural, FTIR and photoluminescence studies of Fe doped ZnO nanopowder by co-precipitation method. *Spect Acta Part A Mol Biomol Spectrosc* 131:185
- [37] Ahsanulhaq Q, Kim JH, Lee JS, Hahn HB (2010) Electrical and gas sensing properties of ZnO nanorod arrays directly

- grown on a four-probe electrode system. *Electrochem Commun* 12:477
- [38] Vaseem M, Umar A, Kim SH, Hahn YB (2008) Low-Temperature synthesis of flower shaped CuO nanostructures by solution process: formation mechanism and structural properties. *J Phys Chem C* 112:5735
- [39] Muthukumaran S, Gopalakrishnan R (2012) Structural, FTIR and photoluminescence studies of Cu doped ZnO nanopowders by co-precipitation method. *Opt Mater* 34:1949
- [40] Bhargava R, Sharma PK, Kumar S, Pandey AC, Kumar N (2011) Variation in structural, optical and magnetic properties of $Zn_{1-x}Cr_xO$ ($x = 0.0, 0.10, 0.15$ and 0.20) nanoparticles: role of dopant concentration on non-saturation of magnetization. *Mater Chem Phys* 125:667
- [41] Vempati S, Shetty A, Dawson P, Nanda KK, Krupanidhi SB (2012) Solution-based synthesis of cobalt-doped ZnO thin films. *Thin Solid Films* 524:138
- [42] Yang C, Su X, Xiao F, Jian J, Wang J (2011) Gas sensing properties of CuO nanorods synthesized by a microwave-assisted hydrothermal method. *Sens Actuators B Chem* 158:301
- [43] Hassan MM, Khan W, Azam A, Naqvi AH (2015) Influence of Cr incorporation on structural, dielectric and optical properties of ZnO nanoparticles. *J Ind Eng Chem* 21:290
- [44] Li T, Qiu H, Wu P, Wang M, Ma R (2007) Characteristics of Ni doped ZnO: Al films grown on glass by direct current magnetron co-sputtering. *Thin Solid Films* 515:3908
- [45] Koseoglu Y (2014) A simple microwave-assisted combustion synthesis and structural, optical and magnetic characterization of ZnO nanoplatelets. *Ceram Int* 40:4676
- [46] Wang Y, Jiang T, Meng D, Wang D, Yu M (2015) Synthesis and enhanced photocatalytic property of feather like Cd-doped CuO nanostructures by hydrothermal method. *Appl Surf Sci* 355:195
- [47] Foo KL, Kashif M, Hashim U, Ali ME (2013) Fabrication and Characterization of ZnO thin films by Sol-gel spin coating method for the determination of phosphate buffer saline concentration. *Curr Nanosci* 9:000
- [48] Yosif AA (2014) Structural and electrical characterization of ZnO and ZnO: Co nano-particles grown on p-Si prepared by PLD. *Int J Emerg Trends Technol Comput Sci* 3:167
- [49] Jeyarani WJ, Tenkyong T, Bachan N, Kumar DA, Shyla JM (2016) An investigation on the tuning effect of glucose-capping on the size and bandgap of CuO nanoparticles. *Adv Power Technol* 27:345
- [50] Samarasekera P, Wijesinghe U, Jayaweera EN (2015) Impedance and electrical properties of Cu doped ZnO thin films. *GESJ Phys* 1(13):5
- [51] Tewari S, Bhattacharjee A (2011) Structural, electrical and optical studies on spray-deposited aluminium-doped ZnO thin films. *Pramana J Phys* 76:158
- [52] Salina M, Ahmad R (2012) Bandgap alteration of transparent zinc oxide thin film with Mg dopant. *Trans Electr Electron Mater* 13:68
- [53] Yathisha RO, Arthoba Nayaka Y, Vidyasagar CC (2016) Microwave combustion synthesis of hexagonal prism shaped ZnO nanoparticles and effect of Cr on structural, optical and electrical properties of ZnO nanoparticles. *Mater Chem Phys* 181:174